# FIRING TESTS ON CLAY-RICH RAW MATERIALS FROM THE ALGARVE BASIN (SOUTHERN PORTUGAL): STUDY OF MINERAL TRANSFORMATIONS WITH TEMPERATURE

MARIA JOSÉ TRINDADE[1,4,*], MARIA ISABEL DIAS[1,4], JOÃO COROADO[2,4], AND FERNANDO ROCHA[3,4]

[1] Instituto Tecnológico e Nuclear EN 10, 2686-953 Sacavém, Portugal
[2] Departamento Arte, Conservação e Restauro, Instituto Politécnico de Tomar, 2300-313 Tomar, Portugal
[3] Departamento de Geociências, Universidade de Aveiro, Campus de Santiago, 3810-193 Aveiro, Portugal,
[4] GeoBioTec − GeoBiociências, Geotecnologias e GeoEngenharias, Universidade de Aveiro, Portugal

**Abstract**—In cases where the provenance of raw materials used in the manufacture of local archeological ceramics is of interest, a detailed study of thermal transformations of minerals may be useful. The purpose of this study was to measure mineralogical transformations of different types of clays obtained during experimental firing runs, carried out at different temperatures, with the main goal of establishing Algarve reference groups based on the composition of raw material and high-temperature mineralogy, which may be compared with ceramics in studies of provenance. Eleven samples of clay-rich raw materials from the Algarve Basin (southern Portugal) were fired to temperatures ranging from 300 to 1100ºC in increments of 100ºC under oxidizing conditions. These were chosen to have variable chemical and mineralogical compositions, representing the main compositional range of the clay deposits from the region. Mineralogical and geochemical characterizations of the original clays were carried out by X-ray diffraction (XRD) and X-ray fluorescence (XRF), respectively. Mineral transformations on the fired products were also studied by XRD.

Three groups of clays were distinguished according to the type of neoformed high-temperature minerals: (1) non-calcareous clays; (2) clays containing calcite as the only carbonate; and (3) clays with dolomite or dolomite + calcite. Firing of non-calcareous clays produced mullite at 1100−1200ºC. Gehlenite and wollastonite formed by firing calcite-rich clays above 900ºC, accompanied by anorthite or larnite in samples with small or large calcite contents, respectively. Firing of dolomite-rich clays at temperatures >900ºC yielded a member of the gehlenite−åkermanite group and diopside. Anorthite, enstatite, periclase, forsterite, and monticellite may also form in the firing products.

**Key Words**—Algarve Basin, Clays, Firing Tests, High-temperature Minerals, Mineral Transformations, X-ray Diffraction.

## INTRODUCTION

The existence in the Algarve of several centers of production of ceramics (local kilns) of Roman age (Vasconcellos, 1898, 1920; Maia, 1979; Alves *et al.*, 1990; Arruda and Fabião, 1990; Fabião, 2004; Viegas, 2006) makes this region an interesting place to study the possible raw materials used in the manufacture of local archeological ceramics, in order to establish their provenance. The classical approach to provenance studies uses geochemical analysis combined with multivariate statistical analysis. In addition to this, study of the mineral transformations of regional clays induced by firing and their comparison with the mineralogical composition of shards may help to determine the type of clay used and the temperatures to which they may have been exposed during production. In such a comparison one must take into account that ceramics are not merely fired clays and their composition depends not only on the chemical and mineralogical composition of the clays, but also on the grain-size distribution, the possible addition of different types of non-plastic grains as temper, the mixture of clays, the firing process, the maximum heating temperature reached in the kiln, the heating ratio, the duration of firing, the kiln redox atmosphere, and the post-depositional alteration (Maggetti, 1982; Rice, 1987; Moropoulou *et al.*, 1995; Velde and Druc, 1999).

In the present work the mineral transformations with increasing temperature for 11 clays of Carboniferous to Holocene age, from the Algarve region, were compared. The main goal was to study the mineral transformations of natural clays with increasing temperature and to establish reference groups based on raw-material composition and high-temperature mineralogy.

Holding all experimental conditions constant except temperature, any differences at discrete temperature steps are assumed to be due to differences in the original samples. Tabulation of these differences may be used to compare shards from the local Roman kilns in order to help determine their provenance and the maximum temperatures reached during their manufacture. This

* E-mail address of corresponding author:
mjtrindade@itn.pt

complements archeometric work already developed in amphora production from the Algarve region (Dias *et al.*, 2009; and other studies in preparation).

## GEOLOGIC CONTEXT

The Algarve basin (Figure 1) located in southern Portugal comprises Triassic to Holocene sediments on a basement of low-grade Carboniferous slates and greywackes (Munhá, 1990) deformed during the Iberian Variscan orogen (Oliveira, 1990).

Sedimentation in the basin was controlled by extensional tectonics associated with the breakup of Pangea, from Lower Triassic to Upper Cretaceous times (Terrinha, 1998). The Cenozoic record probably started in the Lower Miocene (Cachão, 1995) in a basin superimposed on a Mesozoic basin (Terrinha, 1998). The hiatus separating the two basinal cycles corresponds to the main phase of tectonic inversion and uplift of the Mesozoic rift basin (Terrinha, 1998).

Sedimentary environments evolved from continental in the Triassic through confined littoral and evaporitic in Upper Triassic-Hettangian to Sinemurian times, to open marine in the Early Pliensbachian (Terrinha *et al.*, 2006). Triassic sediments consist of red terrigenous siliciclastics (conglomerates, arenites, and shales); Upper Triassic−Hettangian to Sinemurian sediments consist of red shales, dolomites, and evaporites; and Early Pliensbachian sediments consist of limestones, dolomites, and marls. The rifting phase was accompanied by

a tholeiitic volcanic event at the Hettangian−Sinemurian transition (Martins, 1991; Martins and Kerrich, 1998), which formed a volcano-sedimentary complex composed mainly of basaltic lavas and pyroclastic rocks intercalated with clays, dolomites, or limestones.

During the Jurassic and Cretaceous the sedimentation was essentially marine (limestones and marls predominate) characterized by facies variations, triggered by more or less pronounced sea-level fluctuations. Transgression cycles of the Lower Cretaceous were sometimes interrupted by intense tectonic movements, which were responsible for siliciclastic fluvial discharges (Terrinha *et al.*, 2006).

After the period of intense tectonics from Upper Cretaceous to Early Miocene, sedimentary deposition occurred during two transgression cycles (Middle and Upper Miocene) separated by a hiatus that represents a generalized uplift of the Algarve sector (Cachão and Silva, 1992). The first sequence of sediments is carbonate-rich and the second is arenitic (Cachão *et al.*, 1998; Terrinha *et al.*, 2006).

Pliocene to Pleistocene detrital sediments fossilize the karstified Jurassic to Miocene carbonate series. Holocene deposition was influenced by frequent climatic oscillations and sea-level fluctuations (Moura *et al.*, 2007), forming beach sand and dunes that constitute the Ria Formosa island-barrier system, and depositing alluvium terraces and gravels.

Considering this geological diversity and the corresponding occurrence of clay deposits, clay-rich materials
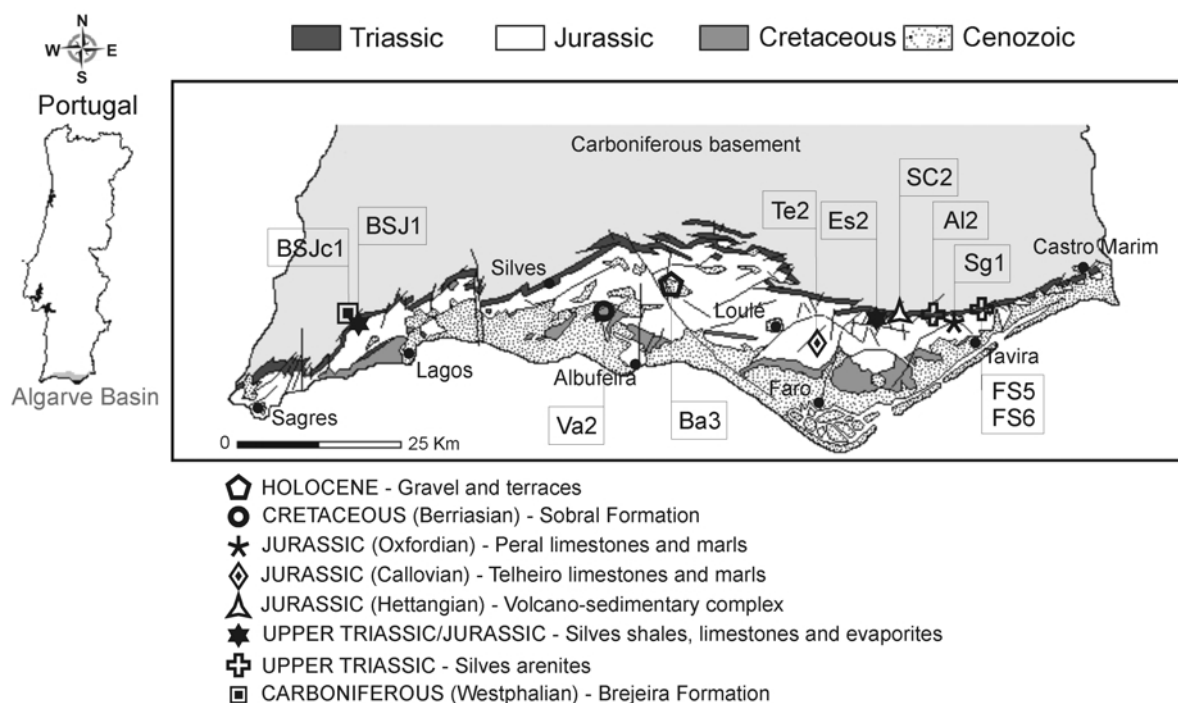


Figure 1. Simplified geologic map of the Algarve Basin showing sample locations.

representative of each clay association were chosen for firing tests and the evaluation of related mineralogical behavior.

## MATERIALS AND METHODS

After a mineralogical and geochemical study of 100 clay samples from the main clay deposits of Algarve, 11 samples representing the observed compositional variability were selected for firing experiments to simulate the ceramic manufacture process following Trindade (2007). These were distributed over a large geographic area and included eight geological units (Figure 1). The main compositional criteria were related to the presence/absence of carbonates, their abundance and composition (calcite or dolomite), the relative proportions of quartz and phyllosilicates (clay minerals), and the presence/absence and type of Fe-rich minerals (goethite or hematite).

To make the test pieces, ~150 g of each sample was pulverized in a mill with an agate ring mortar and homogenized mechanically in a Turbula T2C mixer for 2 h. From each powdered sample, nine portions of 10 g each were placed in plastic containers and pressed at 1200 kg/cm$^2$ in a Specac hydraulic press (Specac Ltd., Orpington, Kent, UK). This produced cylindrical test pieces of 4 cm × 0.3 cm (diameter × height).

Firing tests were performed at the 'Centro Tecnológico da Cerâmica e do Vidro,' Coimbra (Portugal). The test pieces were dried at 110ºC and heated at 300, 400, 500, 600, 700, 800, 900, 1000, and 1100ºC in an oxidizing atmosphere. Non-carbonate samples were also fired subsequently at 1200ºC to allow confirmation of mullite crystallization. The firing cycle in the electric kiln was 5ºC/min and was kept at maximum temperature for 30 min.

Chemical analysis of major oxides of the unfired clays was carried out by XRF at the 'Departamento de Geociências, Universidade de Aveiro' (Portugal). A 1:9 sample to flux (Spectromelt A12) (Merck, KGaA, Darmstadt, Germany) ratio was fused to a glass bead and then analyzed with a Philips PW 1410/00 spectrometer (PANalytical B.V., Almelo, The Netherlands), using CrKα radiation. The Na$_2$O and K$_2$O contents were determined by flame photometry, using a Corning 400 spectrometer (Corning Ltd, Halstead, Essex, UK). Loss on ignition was determined by weighing the samples before and after heating at 1000ºC for 3 h.

X-ray diffraction (XRD) was used to determine the bulk mineralogy and the clay mineral assemblages of the original clays and to characterize the high-temperature phases obtained after firing. The XRD analysis was performed at the 'Instituto Tecnológico e Nuclear' (Portugal), using a Philips X'Pert Pro diffractometer, with a PW 3050/6x goniometer, CuKα radiation, and operating at 45 kV and 40 mA. The mineralogy was determined on powder samples in the 4−60º2θ range,

using a fixed divergence slit with 1º size, a step size of 0.02º2θ, and a scan time of 1.25 s per step.

The clay mineralogy was determined on oriented preparations of the <2 μm fraction after air-drying, heating to 550ºC, and ethylene-glycol solvation. The XRD patterns were obtained in the 2−30º2θ range, using a 1/2º divergence slit and other conditions identical to those used in unoriented preparations. The samples were treated with acetic acid and sodium acetate buffer solution at pH = 5 to remove the carbonates and then washed with distilled water and centrifuged several times. The >63 μm sand fraction was separated by wet sieving of the dispersed material using distilled water and finally the <2 μm clay fraction was separated by gravity settling in water, according to Stokes' law. Oriented slides were prepared by pipetting a small amount of clay suspension onto a glass slide and leaving to dry at room temperature.

Semi-quantitative analysis of the unfired clays was achieved measuring the diagnostic peak areas, considering the full width at half maximum (FWHM), and then weighted by empirical factors according to Schultz (1964), Biscaye (1965), Martín Pozas (1968), Galhano *et al.* (1999), and Oliveira *et al.* (2002) (Table 1). The total proportion of clay minerals in each sample was first determined by considering the peak area of the diffraction maximum of the phyllosilicates at 4.48 Å in unoriented preparations. The percentages of the different clay minerals were then obtained from the peak areas of the diagnostic basal reflections of the species in the glycolated clay fractions.

Based on the XRD data, a synthesis table of the mineral transformations in each sample was constructed

Table 1. List of reflection powers (RP) used for semi-quantification of minerals in unoriented aggregates (bulk mineralogy) and oriented aggregates (clay mineralogy).

| Mineral | RP |
|---|---|
| Unoriented mounts | |
| Quartz | 2 |
| Phyllosilicates | 0.1 |
| Calcite | 1 |
| Dolomite | 1 |
| Alkali feldspar | 1 |
| Plagioclase | 1 |
| Hematite | 1.3 |
| Goethite | 1.3 |
| Anatase | 1 |
| Rutile | 1 |
| Anhydrite | 1.5 |
| | |
| Oriented mounts | |
| Illite | 0.5 |
| Kaolinite | 1 |
| Smectite | 4 |
| Chlorite | 1.25 |

(Table 2). This table describes the rate of diminishing/ disappearance of original minerals, the formation temperature of the high-temperature phases, and the temperature at which they acquire maximum abundance. The peak heights (counts) of the main reflection of each mineral, at each temperature, were registered and transformed so that the sum height of all minerals was equal to 100%. This transformation step is necessary because the peak height may depend on several factors such as the initial sample quantity, the percentage of the vitreous phase, and also on the orientation of crystals. Because the original minerals tend to disappear with increasing temperature and new minerals form after a certain temperature, in Table 2 the unfired specimens were considered as the maximum abundance (or 100%) and the height values of the fired specimens were converted to relative percentages. For each neoformed mineral an abundance of 100% was attributed to the fired specimen with the largest height value, and the proportions of that mineral in the remaining fired specimens were then converted to percentages.

## RESULTS AND DISCUSSION

As the main goal of this work was to identify neoformed minerals diagnostic of the presence of certain original minerals and the range of temperatures over which they were formed, the following discussion is based on groups of clays with similar initial compositions. The firing behavior of non-calcareous and calcareous raw materials is considerably different (Peters and Iberg, 1978; Duminoco *et al.*, 1998; Riccardi *et al.*, 1999; Cultrone *et al.*, 2001; Jordán *et al.*, 2001; Traoré *et al.*, 2003; Trindade *et al.*, 2009) and, in the second group of materials, the carbonate composition influences the formation of minerals at high temperatures, as shown in $Al_2O_3$-CaO-$SiO_2$ (A-C-S) and MgO-CaO-$SiO_2$ (M-C-S) systems (Figure 2).

In the A-C-S system all non-calcareous clays lie on the A-S line; as a result they could only produce high-temperature phases such as mullite. The presence of Ca in the calcareous clays enables the neoformation of gehlenite, anorthite, and wollastonite among others, depending on the relative proportions of the three components and the temperature of firing. In the M-C-S system, calcareous clays are separated into two groups based on the type of carbonate: one group consisting of samples with calcite and the other consisting of samples with dolomite, with/without calcite. The presence of CaO and MgO produces much more complex mineral transformations during firing.

The synthesis of results (Tables 2, 3, and 4; Figures 3−6) in terms of the composition of starting clays and the mineralogical transformations with temperature, and the related discussion, is based on the three groups of raw materials defined above: (1) non-calcareous clays; (2) clays containing calcite as the only carbonate; and (3) clays with dolomite or dolomite + calcite.

The mineral abbreviations listed in Table 5 are used throughout this work.

### Non-calcareous clays

Three non-calcareous clays were studied: (1) sample BSJc1 from the Brejeira Formation (Carboniferous), a residual clay resulting from weathering of slates of the Baixo Alentejo Flysch. The sample was collected from an inactive clay pit in Barão de São João (Lagos); (2) sample Va2 from the Sobral Formation (Berriasian, Lower Cretaceous), which came from Vales nº 5 clay pit (Algoz); and (3) sample Ba3 from gravel and terraces unit (Holocene), collected in the inactive clay pit of Barreiros (Paderne).

*Mineralogical and chemical composition of the clays.* The samples consist mainly of quartz and phyllosilicates in variable amounts, with the phyllosilicate/quartz ratio being greater for BSJc1 (= 2.2) than for Va2 (= 0.5)
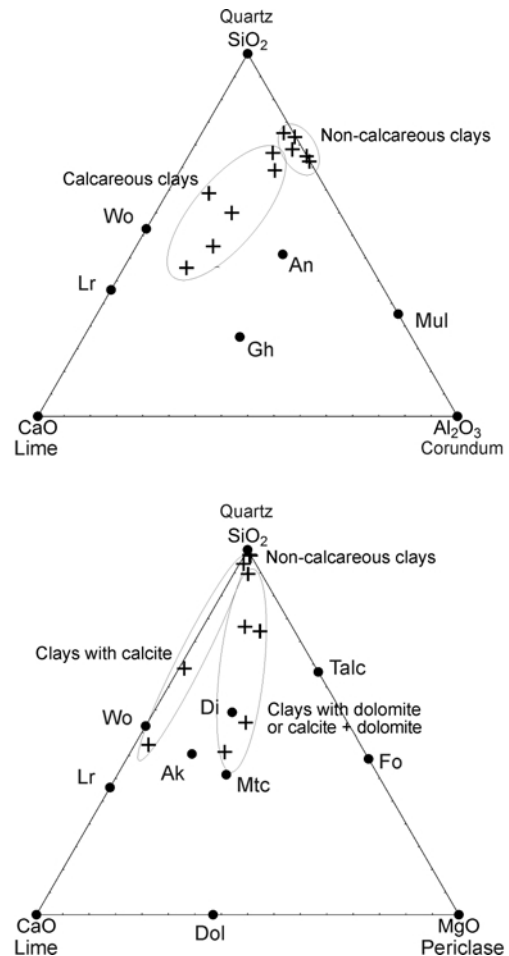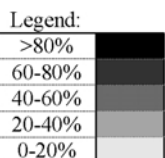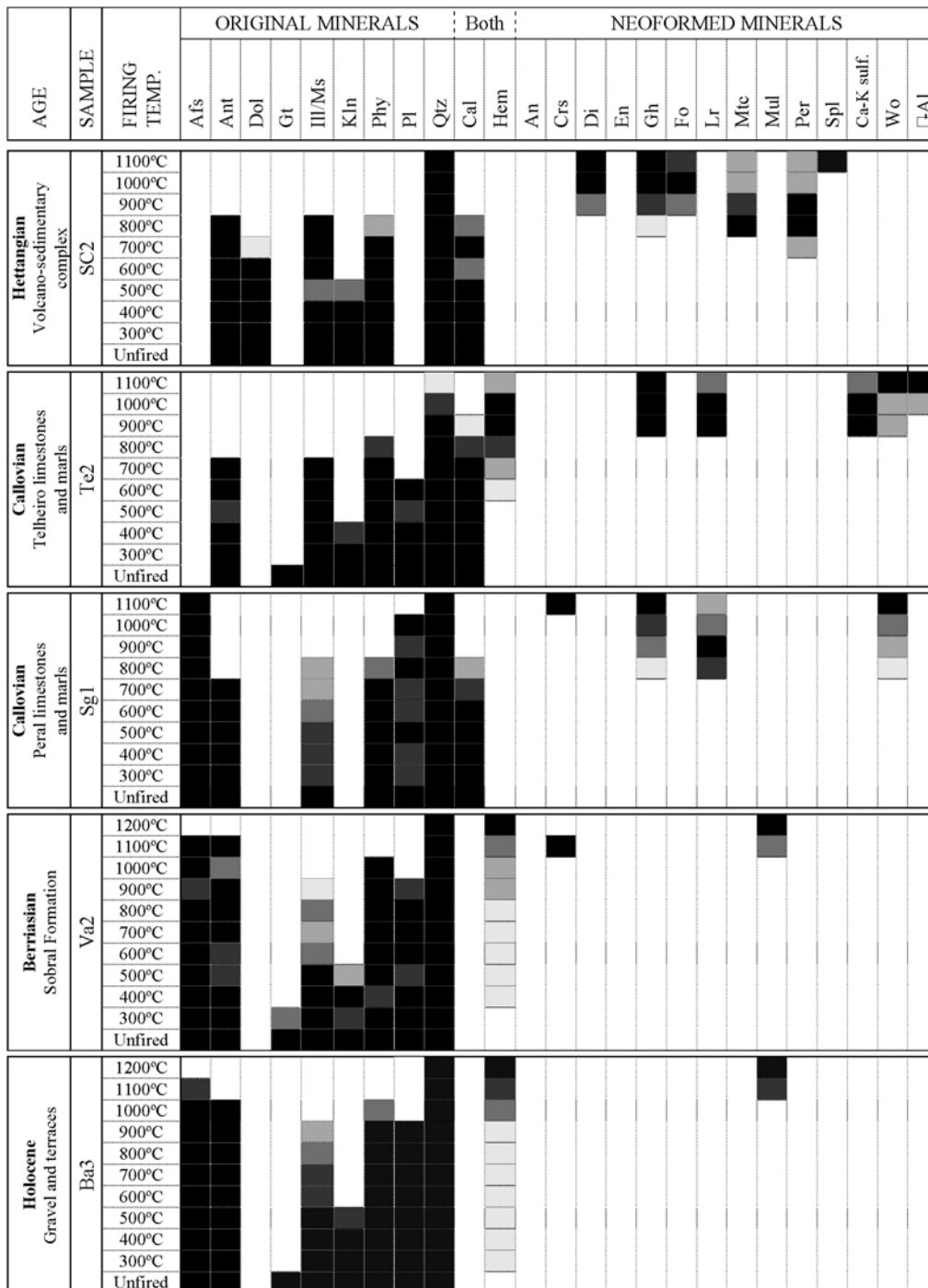


Figure 2. $Al_2O_3$–CaO–$SiO_2$ (A-C-S) and MgO–CaO–$SiO_2$ (M-C-S) triangular diagrams reporting the bulk compositions of the clay samples (+) and ideal phases (filled circles).

Table 2. Synthesis of the mineralogical transformations for each sample after the firing tests. Abbreviations listed in Table 5.

Table 2(*contd.*).



Legend:

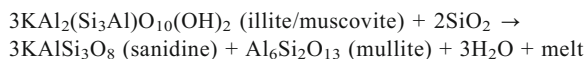| | |
|---|---|
| >80% | ■ |
| 60-80% | ■ |
| 40-60% | ■ |
| 20-40% | ■ |
| 0-20% | ■ |

(Table 3, Figure 3). Anatase, alkali feldspar, plagioclase, goethite, and rutile were found in trace amounts. Clay mineral assemblages were composed mostly of illite and lesser amounts of kaolinite. Chlorite and smectite were also identified in samples BSJc1 and Ba3, respectively.

The chemical composition (Table 4, Figure 3) shows large $SiO_2$ and $Al_2O_3$ contents, with a $SiO_2/Al_2O_3$ ratio varying from 2.6 to 3.4 in BSJc1 and Va2, respectively. The samples have relatively large $Fe_2O_3$ contents (7−8.5%) and $TiO_2$ contents (1.1−1.2%) that are mostly present as goethite and anatase/rutile. A large $K_2O/Na_2O$ (= 4−11) ratio is also observed, which is attributed to the illitic composition of the clays. The absence of carbonates is reflected in the very small percentages of CaO and MgO; therefore, the loss on ignition values reflect dehydroxylation of the clay minerals.

*Mineral transformations during firing.* The first mineral transformations (Table 2, Figure 3) observed with increasing temperature included the dehydroxylation of goethite at 300−400ºC, followed by kaolinite, which diminished abruptly between 400 and 500ºC and was absent at higher temperatures. Illite, which transformed to muscovite with increasing temperature, was observed at up to 1000ºC, as also shown by the peak at 4.48 Å. Generally, plagioclase disappeared before 1000ºC, anatase and alkali feldspars seemed to persist up to 1000−1100ºC, and quartz was preserved even at 1200ºC. Feldspars (especially alkali feldspars) are fluxes, so they may be neoformed during firing because at 800−1000ºC illite/muscovite undergoes a solid-state phase change to mullite and K-feldspar (sanidine), plus a melt, according to the following reaction (Cultrone *et al.*, 2001):

$$3KAl_2(Si_3Al)O_{10}(OH)_2 \text{ (illite/muscovite)} + 2SiO_2 \rightarrow$$
$$3KAlSi_3O_8 \text{ (sanidine)} + Al_6Si_2O_{13} \text{ (mullite)} + 3H_2O + \text{melt}$$

Despite firing, the quartz observed was α-quartz. As the α−β inversion occurs upon heating above a critical temperature the opposite is also true; the process is reversible or irreversible, depending on the heating rate. Because XRD was only carried out after slow cooling to room temperature, the observed quartz is in fact a low quartz pseudomorph after β-quartz (Wahl *et al.*, 1961).

The neoformed mineralogy is relatively simple, consisting of hematite and mullite. Hematite resulted from dehydroxylation of goethite by the reaction $2FeOOH \rightarrow Fe_2O_3 + H_2O$ (Brindley and Brown, 1980), firstly poorly ordered (500−900ºC) and then well ordered up to 1200ºC. Mullite appeared at 1100ºC, and its abundance increased at higher temperatures. Cristobalite was identified only in the quartz-rich Va2 at 1100ºC.

Mullite formed directly from metakaolinite, a dehydroxylized product of kaolinite, by the reactions (Okada and Otsuka, 1986; Murad and Wagner, 1998; Chen *et al.*, 2000):

Table 3. Mineral assemblages (wt.%) of the clay-rich materials.

| Sample | Bulk mineralogy | | | | | | | | | | | Clay mineralogy | | | | |
| --- | Qtz | Phy | Cal | Dol | Afs | Pl | Hem | Gt | Ant | Rt | Anh | Ill | Kln | Sme | Chl | Other |
| BSJc1 | 28 | 62 | – | – | 2 | 1 | – | 1 | 5 | 1 | – | 79 | 17 | – | 4 | – |
| Al2 | 63 | 21 | 7 | – | 3 | 1 | 3 | – | – | – | 2 | 91 | 9 | tr | – | – |
| FS6 | 16 | 44 | 3 | 30 | 3 | tr | 2 | – | 2 | – | – | 100 | – | – | – | – |
| FS5 | 4 | 48 | – | 45 | – | 1 | 1 | – | 2 | – | – | 100 | – | – | – | – |
| Es2 | 17 | 76 | 1 | 1 | 1 | 1 | 2 | – | 1 | – | – | 99 | 1 | – | – | – |
| BSJ1 | 35 | 37 | 8 | 10 | 3 | 3 | 2 | – | 2 | – | – | 87 | – | 7 | 6 | – |
| SC2 | 5 | 49 | 10 | 34 | tr | 1 | – | – | 2 | – | – | 26 | 20 | – | 54 | Chl-Sme |
| Te2 | 7 | 38 | 52 | – | – | 1 | – | 1 | 1 | – | – | 61 | 19 | 13 | 8 | – |
| Sg1 | 28 | 16 | 46 | – | 1 | 7 | – | – | 2 | – | – | 45 | 19 | 36 | – | Ill-Vrm |
| Va2 | 57 | 30 | – | – | 2 | 2 | – | 5 | 2 | 2 | – | 58 | 42 | – | – | – |
| Ba3 | 46 | 48 | – | – | 2 | 2 | – | 1 | 1 | 1 | – | 72 | 21 | 7 | – | – |

Afs − alkali feldspar, Anh − anhydrite, Ant − anatase, Cal − calcite, Chl − chlorite, Chl-Sme − mixed-layer chlorite smectite, Dol − dolomite, Gt − goethite, Hem − hematite, Ill − illite, Ill-Vrm − mixed-layer illite-vermiculite, Kln − kaolinite, Phy − phyllosilicates, Pl − plagioclase, Qtz − quartz, Rt − rutile, Sme − smectite.

Table 4. Chemical composition (wt.%) of the clay-rich materials.

| Sample | $Fe_2O_3$ | MnO | $TiO_2$ | CaO | $K_2O$ | $P_2O_5$ | $SiO_2$ | $Al_2O_3$ | MgO | $Na_2O$ | LOI |
|--------|-----------|-----|---------|-----|--------|----------|---------|-----------|-----|---------|-----|
| BSJc1 | 7.7 | 0.08 | 1.1 | 0.04 | 3.9 | 0.15 | 57 | 22 | 0.9 | 0.36 | 6.6 |
| Al2 | 7.5 | 0.02 | 0.95 | 1.9 | 3.2 | 0.15 | 63 | 16 | 0.64 | 0.47 | 5.3 |
| FS6 | 6.0 | 0.08 | 0.72 | 6.5 | 5.4 | 0.18 | 46 | 15 | 5.8 | 0.20 | 13 |
| FS5 | 3.8 | 0.10 | 0.36 | 16 | 3.4 | 0.09 | 26 | 9.5 | 12 | 0.18 | 28 |
| Es2 | 7.5 | 0.06 | 0.96 | 1.9 | 5.6 | 0.15 | 56 | 18 | 2.1 | 2.0 | 6.7 |
| BSJ1 | 6.5 | 0.14 | 0.76 | 5.1 | 4.0 | 0.19 | 49 | 13 | 8.8 | 0.47 | 11 |
| SC2 | 7.0 | 0.10 | 0.66 | 14 | 0.95 | 0.09 | 30 | 9.8 | 13 | 0.03 | 23 |
| Te2 | 6.5 | 0.05 | 0.46 | 28 | 1.8 | 0.10 | 25 | 9.3 | 1.5 | 0.17 | 27 |
| Sg1 | 2.6 | 0.02 | 0.58 | 21 | 1.2 | 0.04 | 45 | 7.4 | 0.87 | 0.68 | 20 |
| Va2 | 7.0 | 0.06 | 1.2 | 0.17 | 2.5 | 0.03 | 62 | 18 | 0.76 | 0.33 | 6.3 |
| Ba3 | 8.5 | 0.03 | 1.1 | 0.07 | 2.7 | 0.09 | 60 | 18 | 0.95 | 0.68 | 6.8 |

Total Fe as $Fe_2O_3$
LOI = Loss on ignition

$Al_4Si_4O_{10}(OH)_8$ (kaolinite) $\rightarrow$ $Al_4Si_4O_{14}$ (metakaolinite) + $4H_2O$ (~500ºC)

$Al_4Si_4O_{14}$ $\rightarrow$ $Al_4Si_3O_{12}$ (Si-Al spinel) + $SiO_2$ (poorly crystalline) (~925ºC)

$1.5Al_4Si_3O_{12}$ $\rightarrow$ $3Al_2O_3.2SiO_2$ (mullite) + $5SiO_2$ (cristobalite) (~1050−1275ºC)

A transitional aluminous phase (spinel) was not observed, probably due to overlap of the XRD peak with a secondary peak of quartz at 1.98 Å. Mullite formation is expected (A-C-S triangle, Figure 2) not only from decomposition of kaolinite but from all clay minerals. Illite is the main clay mineral in the samples studied, though other effects in the mineralogical transformations with firing have taken place (Aras, 2004; Ferrari and Gualtieri, 2006). Those authors observed a negative correlation between the percentage of illite and that of quartz, cristobalite, and mullite and a positive correlation with the formation of an amorphous phase, due to the intercalated cations, mainly $K^+$ which may act as flux agents. This explains why cristobalite formed only in Va2, which has a large percentage of quartz and a small concentration of illite.

Summarizing, the mineralogy of the fired, non-calcareous clays is very similar; the typical high-temperature phase is mullite though the main mineral in the high-temperature fired specimens is still quartz.

*Clays containing calcite as the only carbonate*

Three samples containing calcite as the only carbonate were studied: (1) sample Al2 from Silves arenites (Upper Triassic), sampled in the Alcarias clay pit (Santa Catarina da Fonte do Bispo); (2) sample Te2 from Telheiro marls unit (Callovian, Middle Jurassic), collected in the Telheiro clay pit near Estói; and (3) sample Sg1 from the Peral marls unit (Oxfordian, Upper Jurassic), sampled in an outcrop near Tavira.

*Mineralogical and chemical composition of the clays.* Sample Al2 contains a large proportion of quartz (>60%), 20% phyllosilicates, a small calcite content (7%), and minor amounts of feldspars, hematite, and anhydrite (Table 3, Figure 4). The most abundant clay mineral is illite, followed by minor amounts of kaolinite and traces of smectite.

Samples Te2 and Sg1 are very rich in calcite (52 and 48%, respectively), and also have large percentages of phyllosilicates, in the case of Te2, and quartz, in the case of Sg1. Minor amounts of quartz, plagioclase, goethite, and anatase were found in Te2 and minor amounts of phyllosilicates, plagioclase, anatase, and alkali feldspar were observed in sample Sg1. The clay mineralogy consists of illite, kaolinite, smectite, and chlorite in Te2 and of illite, smectite, and kaolinite in Sg1.

Samples have variable $SiO_2$ and $Al_2O_3$ contents (Table 4, Figure 4). The siliceous character of Sg1 is well demonstrated by the large $SiO_2/Al_2O_3$ (= 6.1) ratio, whereas Te2 is the least siliceous as shown by the smaller $SiO_2/Al_2O_3$ (= 2.7) ratio. The CaO content, mainly included in calcite, is relatively small (1.9%) in Al2 and very large (>20%) in both of the other two samples, especially in Te2, and justifies the large loss on ignition value obtained. Al2 and Te2 are characterized by large $K_2O/Na_2O$ ratios (6.8 and 10.6, respectively), which indicates the abundance of illite. The $Fe_2O_3$ content of Sg1 (2.6%) is considerably less than that of the other samples (6.5−7.5%).

*Mineral transformations during firing.* Relative to mineral transformations (Table 2, Figure 4) of Al2, kaolinite and plagioclase disappeared at 500ºC and 700ºC, respectively, whereas alkali feldspar was traced up to 1000ºC. Calcite disappeared at 1000ºC. Quartz, phyllosilicates, and hematite were present throughout the entire temperature range, with the abundance of phyllosilicates and hematite being half of the original content at the maximum firing temperature. Neoformed minerals include gehlenite, anorthite, and perhaps wollastonite. Gehlenite appeared at 900ºC and was
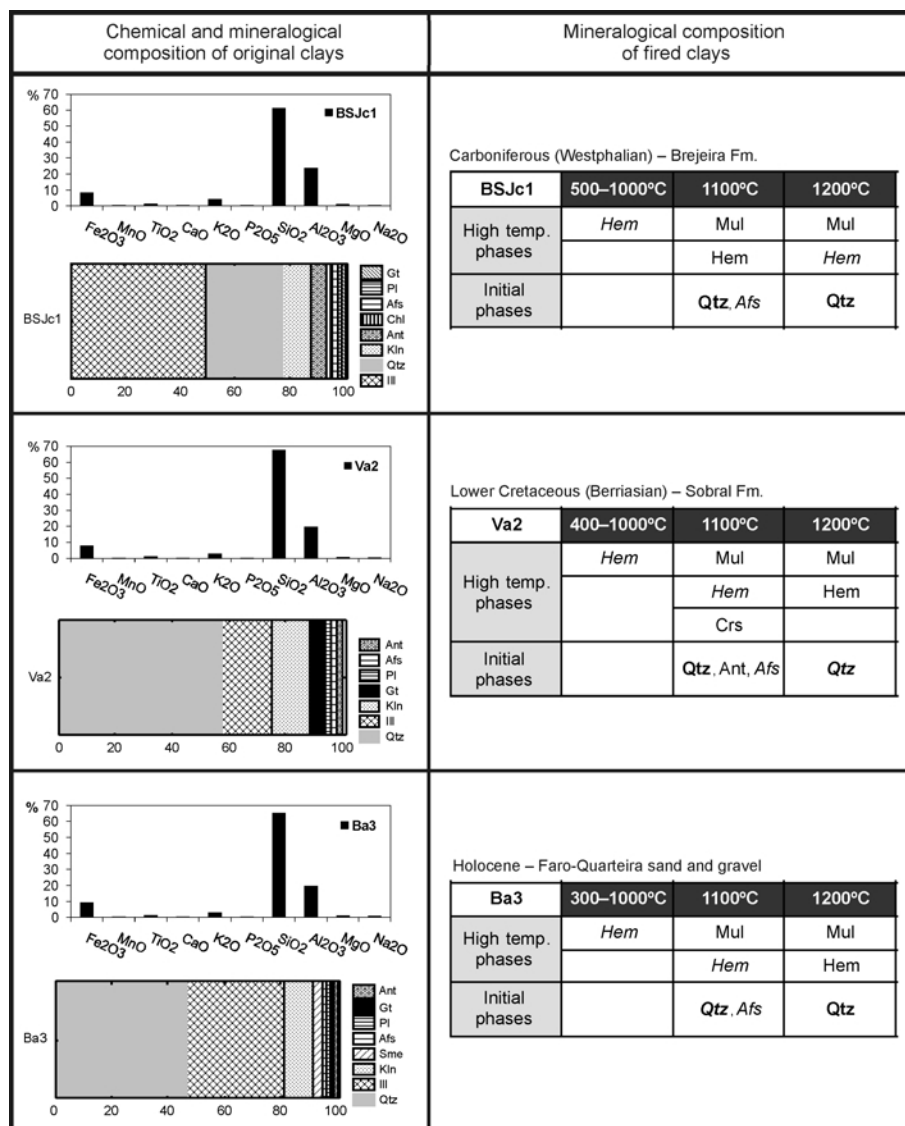
Figure 3. Synthesis of the mineral transformations of non-calcareous clays by firing. The neoformed phases are shown in decreasing abundance for each temperature, determined based on the counting number of the main reflections in XRD patterns, after transformation of the values into percentages to enable comparison between samples. The differences in mineral percentages can be observed in the way in which mineral abbreviations are expressed, according to the scheme: mineral names in **bold**: >50%; mineral names in ***bold italic***: 50–35%; mineral names in regular font: 20–5%; and mineral names in *italic*: <5%. See Table 5 for abbreviations.

most abundant at 1000ºC, whereas anorthite and wollastonite (?) nucleated in very small percentages just before 1000ºC and acquired maximum abundance at 1100ºC.

Te2 mineral transformations with firing included loss of goethite at 300ºC, kaolinite at 500ºC, plagioclase at 700ºC, and anatase and phyllosilicates at 900ºC. Calcite abundance decreased gradually at 800−900ºC and disappeared at 1000ºC. Quartz was retained up to 1100ºC in very small amounts. Hematite was identified

from 600ºC to 1100ºC with maximum abundance at 900−1000ºC and gehlenite, larnite, wollastonite, and a Ca-K sulfate formed at 900ºC. Larnite and Ca-K sulfate were more abundant at 900−1000ºC and wollastonite at 1100ºC. At this high temperature, a transitional alumina phase (γ-alumina) was also observed.

During firing of Sg1, anatase disappeared at 800ºC, phyllosilicates and calcite at 900ºC, and plagioclase at 1100ºC. Alkali feldspar and quartz remained at the highest temperature of firing. Gehlenite and wollastonite

## Chemical and mineralogical composition of original clays / Mineralogical composition of fired clays

**Middle Jurassic (Callovian) – Telheiro limestones/marls**

| Te2 | 500-800°C | 900°C | 1000°C | 1100°C |
|---|---|---|---|---|
| High temp. phases | Hem | Gh | Gh | Gh |
| | | Wo | Wo | Wo |
| | | Hem | Hem | γ-Al |
| | | Lr | Lr | Lr |
| | | Ca-K Sulf. | Ca-K Sulf. | Hem |
| | | | γ-Al | Ca-K Sulf. |
| Initial phases | | Qtz, Cal | Qtz | Qtz |

**Upper Jurassic (Oxfordian) – Peral limestones/marls**

| Sg1 | 800°C | 900°C | 1000°C | 1100°C |
|---|---|---|---|---|
| High temp. phases | Lr | Gh | Gh | Gh |
| | Gh | Wo | Wo | Wo |
| | Wo | Lr | Lr | Lr |
| | | | | Crs |
| Initial phases | Qtz, Cal, Pl, Ms, Afs | Qtz, Pl, Afs | Qtz, Pl, Afs | Qtz, Afs |

**Upper Triassic – Silves arenites**

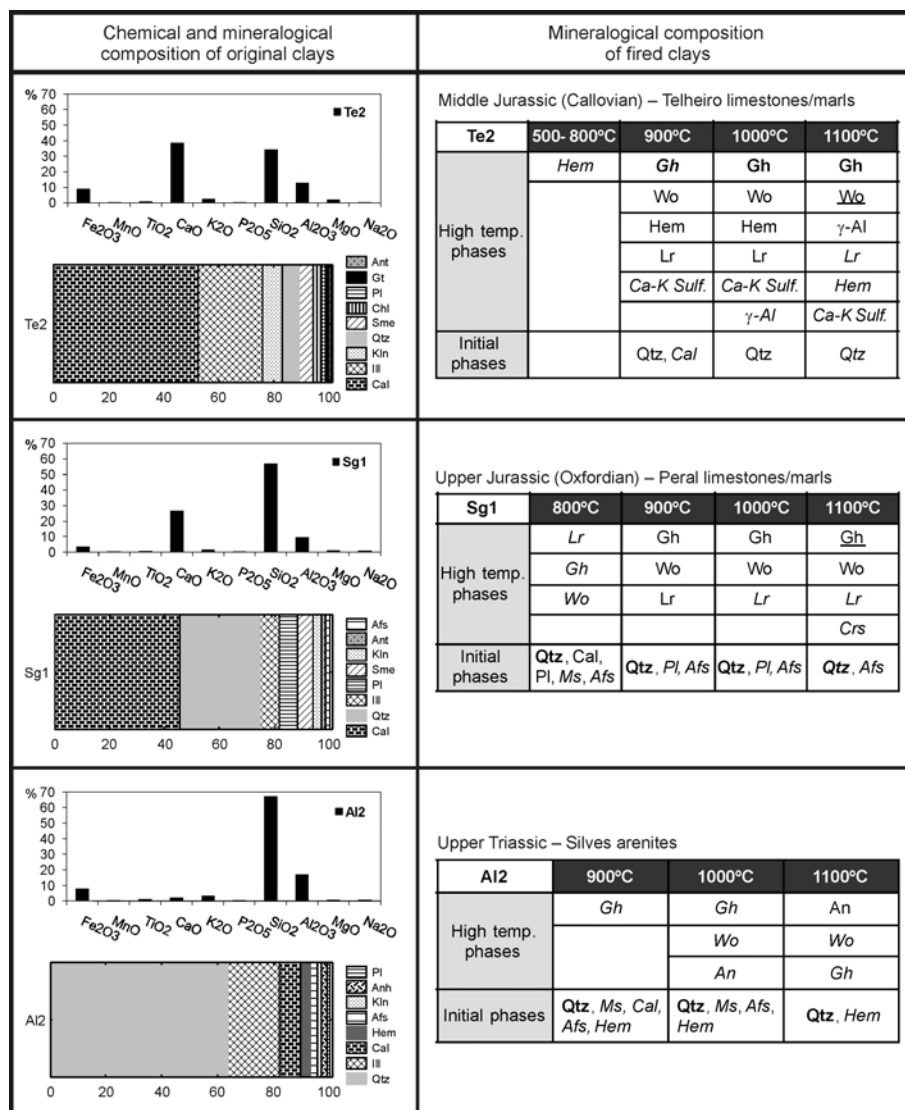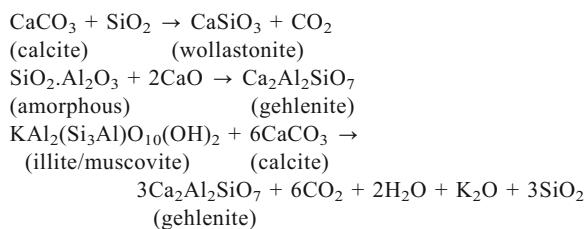| Al2 | 900°C | 1000°C | 1100°C |
|---|---|---|---|
| High temp. phases | Gh | Gh | An |
| | | Wo | Wo |
| | | An | Gh |
| Initial phases | Qtz, Ms, Cal, Afs, Hem | Qtz, Ms, Afs, Hem | Qtz, Hem |

Figure 4. Synthesis of the mineral transformations of clays containing calcite as the only carbonate by firing. The neoformed phases are shown in decreasing abundance for each temperature, determined based on the counting number of the main reflections in XRD patterns, after transformation of the values into percentages to enable comparison between samples. The differences in mineral percentages can be observed in the way in which mineral abbreviations are expressed, according to the scheme: mineral names in **bold**: >50%; mineral names in ***bold italic***: 50–35%; mineral names <u>underlined</u>: 35–20%; mineral names in regular font: 20–5%; and mineral names in *italic*: <5%. See Table 5 for abbreviations.

formed gradually from 800 to 1100°C where they attained maximum abundance. Larnite also started to form at 800°C, acquired maximum abundance at 900°C, and then its concentration diminished, being 20−40% at 1100°C. Cristobalite was detected at 1100°C.

All of the samples studied contain gehlenite and wollastonite, which formed due to the existing $CaCO_3$ in the clays, although some doubts exist as to the presence of wollastonite in sample Al2. These minerals form from reaction of quartz and CaO, in the case of wollastonite, and from reaction of CaO with amorphous compounds which result from dehydroxylation of clay minerals

(Peters and Iberg, 1978; Maniatis *et al.*, 1983; Cultrone *et al.*, 2001), in the case of gehlenite:

$CaCO_3 + SiO_2 \rightarrow CaSiO_3 + CO_2$
(calcite) (wollastonite)
$SiO_2.Al_2O_3 + 2CaO \rightarrow Ca_2Al_2SiO_7$
(amorphous) (gehlenite)
$KAl_2(Si_3Al)O_{10}(OH)_2 + 6CaCO_3 \rightarrow$
(illite/muscovite) (calcite)
$\quad\quad 3Ca_2Al_2SiO_7 + 6CO_2 + 2H_2O + K_2O + 3SiO_2$
(gehlenite)

The presence of lime (CaO), resulting from calcite decomposition, was difficult to confirm in the XRD patterns because its main diffraction peak overlaps a secondary peak of gehlenite, or because the lime may exist as a disordered phase (Peters and Iberg, 1978).

Gehlenite and wollastonite are generally metastable phases that react in the presence of $SiO_2$, producing anorthite as a final phase (Riccardi *et al.*, 1999; Traoré *et al.*, 2000; Jordán *et al.*, 2001); the mechanism to form anorthite, however, is not very clear and at least four reaction schemes have been proposed:
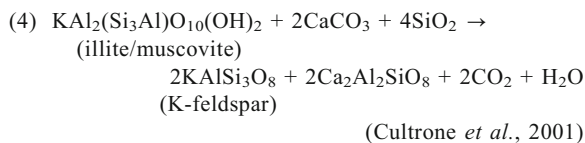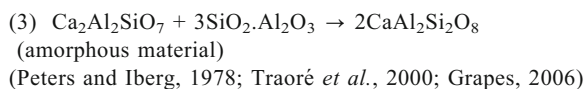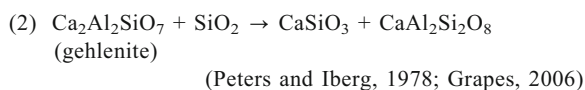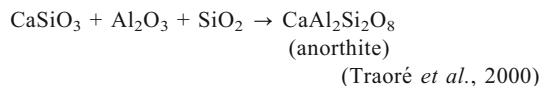
(1)    $CaCO_3 + SiO_2 \rightarrow CaSiO_3 + CO_2$
                         (wollastonite)
and
       $CaSiO_3 + Al_2O_3 + SiO_2 \rightarrow CaAl_2Si_2O_8$
                              (anorthite)
                              (Traoré *et al.*, 2000)

(2)    $Ca_2Al_2SiO_7 + SiO_2 \rightarrow CaSiO_3 + CaAl_2Si_2O_8$
       (gehlenite)
                    (Peters and Iberg, 1978; Grapes, 2006)

(3)    $Ca_2Al_2SiO_7 + 3SiO_2.Al_2O_3 \rightarrow 2CaAl_2Si_2O_8$
 (amorphous material)
(Peters and Iberg, 1978; Traoré *et al.*, 2000; Grapes, 2006)

(4)    $KAl_2(Si_3Al)O_{10}(OH)_2 + 2CaCO_3 + 4SiO_2 \rightarrow$
       (illite/muscovite)
                $2KAlSi_3O_8 + 2Ca_2Al_2SiO_8 + 2CO_2 + H_2O$
       (K-feldspar)
                              (Cultrone *et al.*, 2001)

From (4), the K-feldspar observed after firing at high temperatures is suggested to be a high-temperature phase instead of an original relict phase.

Kacim and Hajjaji (2003) assumed that anorthite may simply form by reaction of CaO with dehydroxylated clay minerals, at least above 1000°C. Nevertheless, anorthite was observed only in Al2. The general absence of anorthite in the samples studied is related to the fact that the type of neoformed minerals depends not only on the temperature but also on silica activity (Riccardi *et al.*, 1999; Kacim and Hajjaji, 2003). The assemblage gehlenite + wollastonite was expected for intermediate $SiO_2$ activities, while the association anorthite + wollastonite developed when $SiO_2$ was abundant.

In Al2, quartz was abundant (>60%) and the calcite content was small (<10%). An increase in anorthite content in specimens fired to 1000−1100°C was accompanied by a significant decrease in the percentage of gehlenite, suggesting the formation of anorthite directly by decomposition of gehlenite.

Samples Te2 and Sg1 contain abundant calcite; therefore the gehlenite + wollastonite association was stable up to high temperatures. The excess CaO enabled the formation of larnite *via* reaction: $2CaO + SiO_2$ (amorphous) $\rightarrow Ca_2SiO_4$.

Cristobalite was also formed in sample Sg1 at 1100°C, probably due to quartz transformation, as was observed by other authors (Benhammou *et al.*, 2009). Cristobalite was not detected in the silica-poor Te2, but some other neoformed minerals, such as Ca-K sulfate and γ-alumina, were identified.

The major original mineral of the high-temperature fired specimens is quartz, which is the most abundant phase in Al2 and Sg1. Due to the large percentage of calcite in Te2, quartz almost disappeared and the main constituent at 900−1100°C is gehlenite. Other original minerals accompanying quartz could be hematite up to 1100°C and plagioclase and muscovite up to 1000°C.

*Clays with dolomite or dolomite and calcite*

Five samples containing dolomite were studied: (1) samples FS5 and FS6 from Silves arenites (Upper Triassic), collected in an outcrop at Fonte Salgada (Tavira); (2) samples Es2 and BSJ1 from the Silves shales, limestones and evaporites unit (Triassic–Hettangian), collected at the Espartosa clay pit (Santa Catarina da Fonte do Bispo) and from an outcrop at Barão de São João (Lagos), respectively; and (3) sample SC2 from the volcano-sedimentary complex (Hettangian, Lower Jurassic), sampled in an outcrop at Santa Catarina da Fonte do Bispo.

*Mineralogical and chemical composition of clays.* Three of the samples (FS5, FS6, and SC2) are very rich in dolomite (30−45%), especially FS5 (Table 3, Figures 5, 6) and consist essentially of illite and dolomite, with lesser quartz and traces of anatase and hematite. Accessory calcite and alkali feldspar were also found in FS6 and SC2. Illite is the only clay mineral in FS5 and FS6, whereas SC2 contains mainly chlorite with minor amounts of illite and kaolinite.

The other two samples (BSJ1 and Es2) have smaller dolomite contents (10 and 1%, respectively) and contain small amounts of calcite. BSJ1 consists mainly of phyllosilicates (illite ± smectite ± chlorite) and quartz in analogous percentages and traces of plagioclase, alkali feldspar, hematite, and anatase. Es2 consists mainly of phyllosilicates (illite ± kaolinite); minor amounts of quartz; and traces of hematite, calcite, dolomite, feldspars, and anatase.

The large dolomite contents of samples FS5, FS6, and SC2 explain the large values of CaO and MgO and, consequently, the large LOI values (Table 4, Figures 5, 6). Those samples have small $SiO_2$ contents (26−46%) and the largest $K_2O/Na_2O$ (19−32) ratio of all the studied clays; the $K_2O$ and $Na_2O$ contents of SC2, however, are much smaller than in the other samples, probably due to the lack of feldspars.

The least carbonated samples (BSJ1 and Es2) have larger $SiO_2$ (49−56%) contents. Sample BSJ1 has a larger $K_2O/Na_2O$ ratio and has greater MgO and CaO contents than sample Es2.

**Chemical and mineralogical composition of original clays**

**Mineralogical composition of fired clays**

*Upper Triassic – Silves arenites*

| FS5 | 600ºC | 700ºC | 800ºC | 900ºC | 1000ºC | 1100ºC |
|---|---|---|---|---|---|---|
| High temp. phases | *Cal* | *Cal* | Per | Gh-Ak | *Gh-Ak* | *Gh-Ak* |
| | | *Per* | Cal | Per | Fo | Fo |
| | | | | Di | Per | Ca-K Sulf. |
| | | | | Ca-K Sulf. | Mtc | Spl |
| | | | | Mtc | Ca-K Sulf. | *Di* |
| | | | | | Di | *Mtc* |
| | | | | | γ-Al | γ-Al |
| | | | | | | Per |
| Initial phases | **Dol**, Qtz, *Ms, Ant, Hem* | **Dol**, Qtz, *Ms, Ant, Hem* | Qtz, Hem, *Ms* | Qtz, Hem, *Ms* | Qtz, Hem | Qtz, Hem |

*Hettangian – Volcano-sedimentary complex*

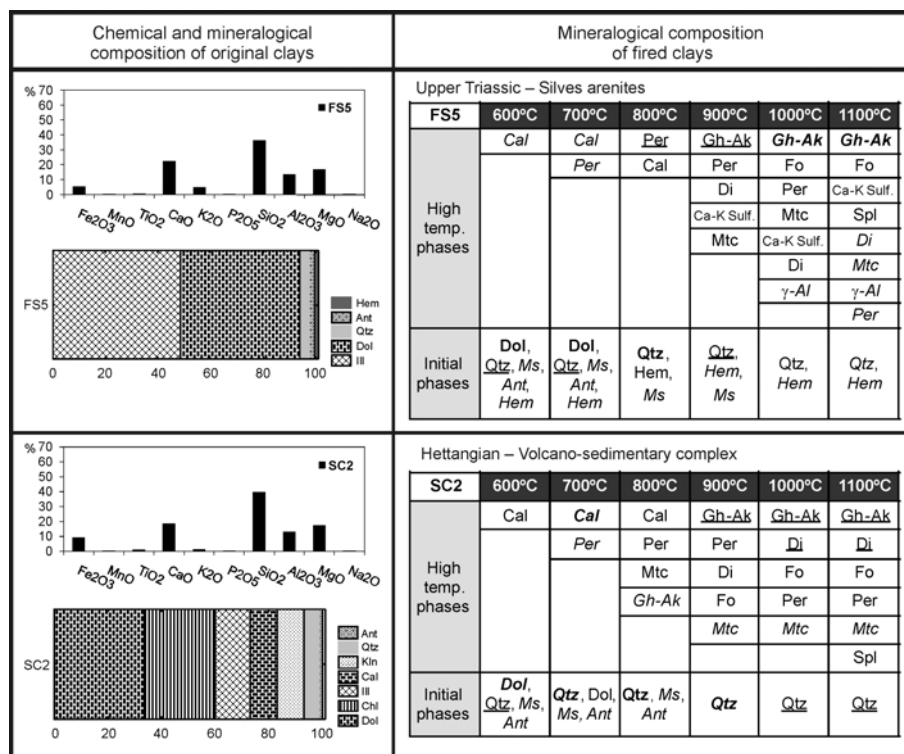| SC2 | 600ºC | 700ºC | 800ºC | 900ºC | 1000ºC | 1100ºC |
|---|---|---|---|---|---|---|
| High temp. phases | Cal | *Cal* | Cal | Gh-Ak | Gh-Ak | Gh-Ak |
| | | *Per* | Per | Per | *Di* | *Di* |
| | | | Mtc | Di | Fo | Fo |
| | | | *Gh-Ak* | Fo | Per | Per |
| | | | | *Mtc* | Mtc | Mtc |
| | | | | | | Spl |
| Initial phases | **Dol**, Qtz, *Ms, Ant* | Qtz, Dol, *Ms, Ant* | Qtz, *Ms, Ant* | **Qtz** | Qtz | Qtz |

Figure 5. Synthesis of the mineral transformations of clays with dolomite or dolomite + calcite by firing. The neoformed phases are shown in decreasing abundance for each temperature, determined based on the counting number of the main reflections in XRD patterns, after transformation of the values into percentages to enable comparison between samples. The differences in mineral percentages can be observed in the way in which mineral abbreviations are expressed, according to the scheme: mineral names in **bold**: >50%; mineral names in ***bold italic***: 50–35%; mineral names underlined: 35–20%; mineral names in regular font: 20–5%; and mineral names in *italic*: <5%. See Table 5 for abbreviations.

*Mineral transformations during firing.* For FS5, anatase and dolomite were the first minerals to disappear at 800ºC. The presence of the diffraction maximum at 4.48 Å up to 900ºC suggests that the phyllosilicates remained up to that temperature. Hematite and quartz were present throughout the temperature range but their abundances decreased at 1100ºC. At 600ºC calcite, resulting from decarbonated dolomite, started to form, increasing in abundance up to 800ºC, after which it disappeared. In this case, calcite is clearly a neoformed phase as it was only observed in the fired specimens. Periclase was observed from 700 to 1100ºC with maximum abundance at 800−900ºC. Diopside, gehlenite, and monticellite appeared at 900ºC, but the diopside content diminished at higher temperatures, and monticellite and gehlenite were more abundant at 1000ºC and 1000−1100ºC, respectively. Forsterite, γ-alumina, and spinel nucleated at 1000−1100ºC. From 900 to 1100ºC a Ca-K sulfate phase was also identified by scanning electronic microscopy (SEM) and XRD observations, as presented by Trindade *et al.* (2009).

The first mineralogical transformation of FS6 was the decrease of dolomite at 800ºC and its disappearance at 900ºC. Calcite disappeared at 900ºC. Due to the presence of calcite and dolomite in the sample, distinction between original and neoformed calcite is difficult. Phyllosilicates and feldspars disappeared before 1000ºC and quartz and hematite were retained at high percentages after firing at 1100ºC. Periclase was first identified at 800ºC and its abundance was at a maximum at 900−1000ºC, decreasing at higher temperatures. Gehlenite was present at 900−1000ºC and forsterite only formed at 1000−1100ºC. Diopside and anorthite appeared at 900ºC and their maximum abundance was observed at 1100ºC.

Relative to SC2, kaolinite was the first mineral to dehydroxylate, disappearing completely at 600ºC. Dolomite diminished abruptly at 700ºC and disappeared at 800ºC. Calcite, phyllosilicates, and anatase were present up to 800ºC and quartz was the only phase at 1100ºC. Regarding the high-temperature phases, periclase was present from 700 to 1100ºC, being most abundant at 800−900ºC. Monticellite appeared at 800ºC where its abundance was at a maximum and then decreased at 1100ºC, while gehlenite also appeared at 800ºC but its content increased up to 1100ºC. Diopside and forsterite were detected at 900−1100ºC, being most abundant at 1000−1100ºC and 1000ºC, respectively. At 1100ºC, traces of a Mg-rich spinel phase were present.
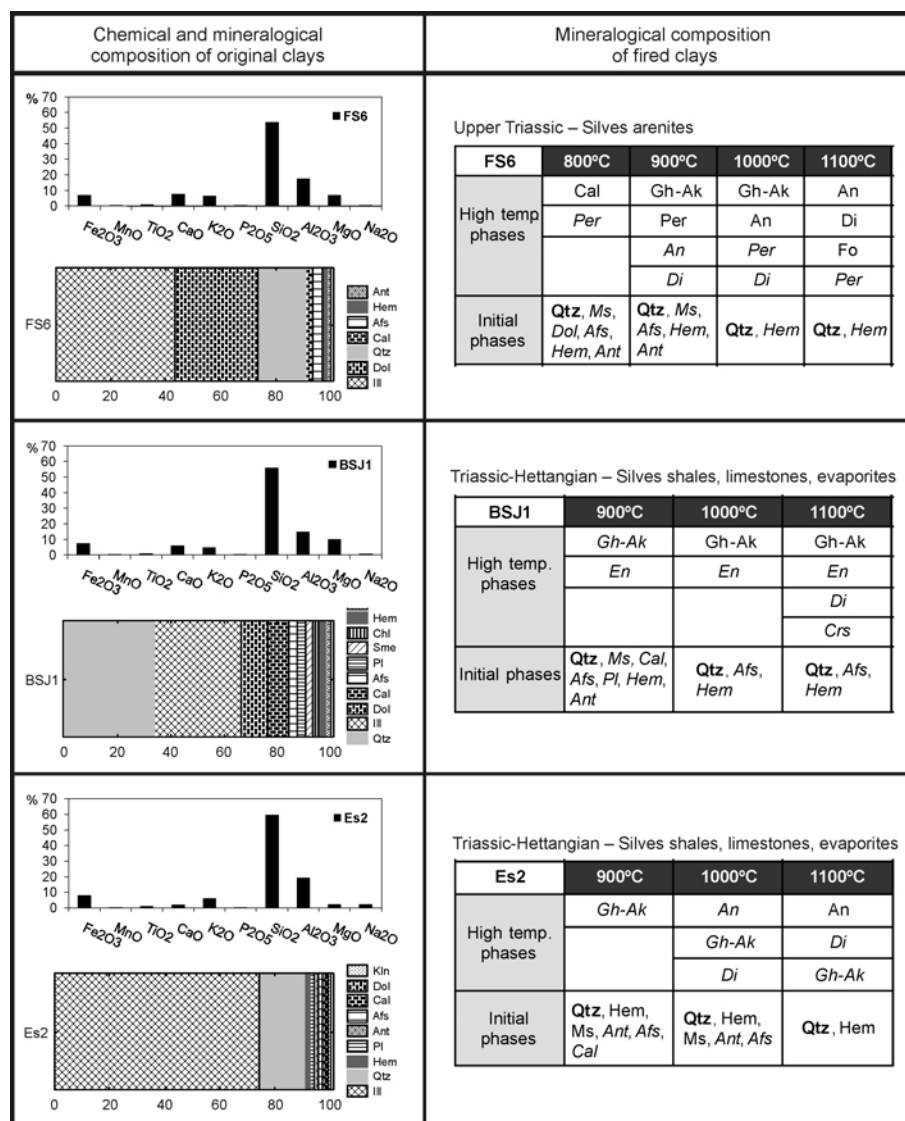
Figure 6. Synthesis of the mineral transformations of clays with dolomite or dolomite + calcite by firing (continuation). The neoformed phases are shown in decreasing abundance for each temperature, determined based on the counting number of the main reflections in XRD patterns, after transformation of the values into percentages to enable comparison between samples. The differences in mineral percentages can be observed in the way in which mineral abbreviations are expressed, according to the scheme: mineral names in **bold**: >50%; mineral names in regular font: 20–5%; and mineral names in *italic*: <5%. See Table 5 for abbreviations.

In BSJ1, traces of dolomite were detected up to 800°C. Calcite decreased abruptly at 800−900°C and disappeared at 1000°C. Anatase, plagioclase, and phyllosilicates were detected up to 900°C and alkali feldspar, quartz, and hematite up to 1100°C. Gehlenite and enstatite appeared at 900°C, being more abundant at 1100°C, where they coexisted with diopside.

In sample Es2, kaolinite and plagioclase disappeared at 600°C and 700°C, respectively. Dolomite and calcite started to decompose at 700°C and 800°C and disappeared at 900°C and 1000°C, respectively.

Phyllosilicates disappeared at 1000°C, anatase and alkali feldspar at 1100°C, and quartz and hematite were present throughout the entire temperature range. High-temperature minerals formed included gehlenite, diopside, and anorthite. Gehlenite appeared at 900°C and its abundance decreased at 1100°C. Anorthite and diopside appeared at 1000°C, and their abundance increased at 1100°C.

Synthesis of the mineral transformations of the dolomite-containing samples (Figures 5 and 6) shows that in dolomite-rich samples (FS5, FS6, and SC2) the

Table 5. List of mineral abbreviations used in this work, their chemical formulae, and the main XRD peaks ($d$ values) used for their identification.

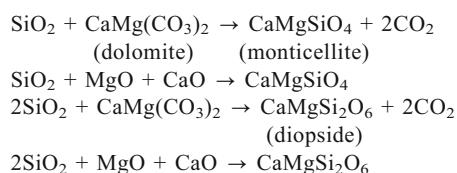| Mineral | Abbreviation | Chemical formula | $d$ (Å) |
|---|---|---|---|
| **Original minerals** | | | |
| Alkali feldspar | Afs | $(K,Na)AlSi_3O_8$ | 3.25 |
| Anatase | Ant | $TiO_2$ | 3.52 |
| Anhydrite | Anh | $CaSO_4$ | 3.50 |
| Dolomite | Dol | $CaMg(CO_3)_2$ | 2.89 |
| Goethite | Gt | $FeO(OH)$ | 4.18 |
| Illite | Ill | $(K,H_3O)(Al,Mg,Fe)_2(Si,Al)_4O_{10}(OH)_2,(H_2O)$ | 10.0 |
| Kaolinite | Kln | $Al_2Si_2O_5(OH)_4$ | 7.18 |
| Phyllosilicates | Phy | $(Si_2O_5^{2-})_n$ | 4.48 |
| Plagioclase | Pl | $(Na,Ca)(Si,Al)_4O_8$ | 3.19 |
| Smectite | Sme | $(Na,Ca)(Al,Mg)_6(Si_4O_{10})_3(OH)_6-nH_2O$ | 17.0 |
| Quartz | Qtz | $SiO_2$ | 3.35 |
| **Original and neoformed** | | | |
| Calcite | Cal | $CaCO_3$ | 3.04 |
| Hematite | Hem | $Fe_2O_3$ | 2.69 |
| **Neoformed minerals** | | | |
| Akermanite | Ak | $Ca_2MgSi_2O_7$ | 2.87 |
| Anorthite | An | $CaAl_2Si_2O_8$ | 3.18 |
| Cristobalite | Crs | $SiO_2$ | 4.05 |
| Diopside | Di | $CaMgSi_2O_6$ | 2.99 |
| Enstatite | En | $MgSiO_3$ | 3.16 |
| Gehlenite | Gh | $Ca_2Al_2SiO_7$ | 2.85 |
| Forsterite | Fo | $Mg_2SiO_4$ | 2.46 |
| Larnite | Lr | $Ca_2SiO_4$ | 2.75 |
| Monticellite | Mtc | $CaMgSiO_4$ | 2.66 |
| Mullite | Mul | $Al_6Si_2O_{13}$ | 3.40 |
| Muscovite | Ms | $KAl_2[(OH)_2AlSi_3O_{10}]$ | 10.0 |
| Periclase | Per | $MgO$ | 2.11 |
| Spinel | Spl | $MgAl_2O_4$ | 2.42 |
| Sulfate (Ca,K) | Ca-K sulf. | ? | 3.13 |
| Wollastonite | Wo | $CaSiO_3$ | 2.98 |
| $\gamma$-Alumina | $\gamma$-Al | $\gamma$-$Al_2O_3$ | 1.98 |

first neoformed mineral is calcite due to decomposition of dolomite. In samples (BSJ1 and Es2) with small abundances of dolomite and calcite, neoformation of calcite is difficult to determine, but in both samples a slight increase in the intensity of the calcite peak occurred at 700ºC. Periclase resulting from decomposition of dolomite was only observed in samples richer in dolomite, especially at 800−900ºC.

Firing caused the decomposition of carbonates, clay minerals, and silicates (feldspars and later, quartz) and the formation of a melt phase rich in Si, Al, Ca, and K (Trindade *et al.*, 2009). From this melt phase, nucleation and crystallization of several metastable phases occurred, continuously reacting with increasing temperature.

The major component of the fired specimens is commonly melilite resulting from reaction of clay minerals and carbonates. Due to the presence of abundant Mg in the system, the melilite formed had åkermanitic composition as was indicated by XRD results, and so was designated the gehlenite−åkermanite phase.

In the dolomite-rich FS5, gehlenite−åkermanite was the main phase in the specimens fired above 800ºC, whereas in samples with smaller initial dolomite/quartz ratios its abundance diminished and quartz became the main component.
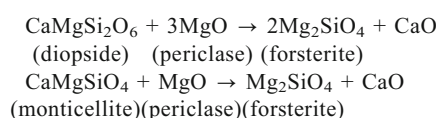
Monticellite and diopside may have crystallized from the vitreous phase or the interfaces between minerals, appearing in their reaction rim, according to the reactions (Miyashiro, 1994; Cultrone *et al.*, 2001; Grapes, 2006):

$$SiO_2 + CaMg(CO_3)_2 \rightarrow CaMgSiO_4 + 2CO_2$$
$$\text{(dolomite)} \qquad \text{(monticellite)}$$
$$SiO_2 + MgO + CaO \rightarrow CaMgSiO_4$$
$$2SiO_2 + CaMg(CO_3)_2 \rightarrow CaMgSi_2O_6 + 2CO_2$$
$$\text{(diopside)}$$
$$2SiO_2 + MgO + CaO \rightarrow CaMgSi_2O_6$$

The crystallization of monticellite started at 800−900ºC and its abundance tended to diminish up to 1100ºC. Monticellite formed in samples (FS5 and SC2) rich in dolomite, containing minor amounts of quartz. On the

contrary, diopside was observed in all samples containing dolomite, even in those with very small amounts of dolomite; diopside is, therefore, probably ubiquitous in clays with dolomite regardless of its abundance, whereas monticellite formed only in clays simultaneously rich in dolomite (high Mg and Ca activities) and with little silica activity, explaining why monticellite was not formed in FS6, despite its large dolomite content.

Because calcite was consumed more rapidly than periclase, the MgO excess combined with $SiO_2$ to form forsterite at 900−1100ºC. Forsterite was generally more abundant at 1100ºC, depending on the composition of the clay; however, given that at 1100ºC the monticellite and diopside contents diminished and the forsterite content increased, the following reactions should also be considered (Miyashiro, 1994; Grapes, 2006):

$$CaMgSi_2O_6 + 3MgO \rightarrow 2Mg_2SiO_4 + CaO$$
(diopside)  (periclase) (forsterite)
$$CaMgSiO_4 + MgO \rightarrow Mg_2SiO_4 + CaO$$
(monticellite)(periclase)(forsterite)

A Mg-rich spinel was also formed at 1100ºC in samples that originally had large dolomite and clay minerals contents. This was probably due to the complete dehydroxylation of clay minerals allied to MgO availability, as suggested by the presence of periclase at 1100ºC. Spinel was formed by the reaction: $MgO + Al_2O_3 \rightarrow MgAl_2O_4$.

In sample BSJ1, originally containing smaller amounts of carbonates, enstatite, gehlenite−åkermanite, and diopside formed from 900 to 1100ºC. The greater Si activity and lesser Mg activity, in comparison to samples FS5, FS6, and SC2, yielded enstatite (Mg:Si = 1:1) instead of forsterite (Mg:Si = 2:1). Enstatite formed according to the reaction: $SiO_2 + MgO \rightarrow MgSiO_3$. The formation of diopside and enstatite by heating clays with small (<10%) dolomite contents has already been reported (Önal *et al.*, 2008).

In the carbonate-poor Es2 sample, the fired specimens consisted mainly of quartz plus hematite. The most abundant neoformed minerals were anorthite, minor diopside, and gehlenite−åkermanite. Comparing this sample, which essentially consists of illite, quartz, and <5% of carbonates, with non-calcareous samples small quantities of carbonates clearly inhibit the formation of mullite and form Ca/Mg rich aluminosilicates, depending on the composition of the carbonate.

## CONCLUSIONS

Different types of clay-rich materials (non-calcareous clays, clays containing calcite as the only carbonate, and clays with dolomite with/without calcite) formed distinct associations of high-temperature phases during firing. The following conclusions are drawn:

(1) Firing non-calcareous raw materials produced mullite after 1000ºC. The presence of small percentages of carbonates inhibited mullite formation and instead Ca-Al silicates (gehlenite and anorthite) were formed.

(2) In clays containing small percentages of carbonates in the form of calcite, the Ca-Al silicates could be accompanied by wollastonite. If dolomite (with/without calcite) was present in the clay, diopside was formed. Gehlenite appeared at 900−1100ºC, whereas anorthite, wollastonite, and diopside were observed at 1000−1100ºC. Quartz remained the main component.

(3) In clays with abundant calcite the typical association of minerals was gehlenite + wollastonite + larnite. Larnite only formed in samples with a large Ca content, where the formation of anorthite was inhibited due to the low silica activity.

(4) The high-temperature products of fired dolomite-rich clays were periclase, monticellite, forsterite, and rarely Mg-rich spinel, minerals which appeared in association with gehlenite−åkermanite and diopside and which crystallized even if the initial dolomite content was small.

(5) The presence of certain high-temperature minerals in the fired specimens is indicative of some raw-material characteristics: gehlenite indicates the existence of carbonates; wollastonite indicates the presence of calcite; larnite indicates large amounts of initial calcite; diopside indicates the presence of dolomite; periclase, monticellite, and forsterite indicate large amounts of initial dolomite.

(6) Where carbonates were abundant they acted as fluxing agents helping to reduce the temperature of first appearance of neoformed minerals, and restricting the temperature range for a vitreous phase due to the formation of a new mineral association at ~900ºC.

Based on raw-material composition and high-temperature mineralogy, the Algarve reference groups were established. Application of the present study will aid future research concerning provenance of locally/regionally produced archeological ceramics.

## REFERENCES

Alves, F.J.S., Diogo, A.D., and Reiner, F. (1990) A propósito dos fornos de cerâmica lusitano-romanos de S. Bartolomeu do Mar. Pp. 193−198 in: *Ânforas lusitanas. Tipologia, produção, comércio* (A. Alarcão and F. Mayet, editors). Museu Monográfico de Conímbriga, Coimbra, Portugal.

Aras, A. (2004) The change of phase composition in kaolinite- and illite-rich clay-based ceramic bodies. *Applied Clay Science*, **24**, 257−269.

Arruda, A.M. and Fabião, C. (1990) Ânforas da Quinta do Lago (Loulé). Pp. 199−213 in: *Les amphores Lusitaniennes.*

*Typologie, Production, Commerce* (A. Alarcão and F. Mayet, editors). De Bocard, Paris.

Benhammou, A., Tanouti, B., Nibou, L., Yaacoubi, A., and Bonnet, J.-P. (2009) Mineralogical and physicochemical investigation of Mg-smectite from Jbel Ghassoul, Morocco. *Clays and Clay Minerals*, **57**, 264–270.

Biscaye, P.E. (1965) Mineralogy and sedimentation of recent deep-sea clay in the Atlantic Ocean and adjacent seas and oceans. *Geological Society of America Bulletin*, **76**, 803–832.

Brindley, G.W. and Brown, G. (1980) *Crystal Structures of Clay Minerals and their X-ray Identification*. Monograph **5**, Mineralogical Society, London.

Cachão, M. (1995) Utilização de nanofósseis calcários em biostratigrafia, paleocenografia e paleocologia. Aplicações ao Neogénico do Algarve (Portugal) e do Mediterrâneo Ocidental (ODP 653) e a problemática de Coccolithus pelagicus. PhD thesis, University of Lisbon, Portugal, 450 pp.

Cachão, M. and Silva, C.M. (1992) Neogene palaeogeographic evolution of Algarve Basin (southern Portugal): a two step model. Preliminary data. *Gaia*, **4**, 39–42.

Cachão, M., Boski, T., Moura, D., Dias, R.P., Silva, C.M., Santos, A., Pimentel, N., and Cabral, J. (1998) Proposta de articulação das unidades sedimentares neogénicas e quaternárias do Algarve (Portugal). Actas do V Congresso Nacional de Geologia. *Comunicações do Instituto Geológico e Mineiro*, **84**, A169–A172.

Chen, C.Y., Lan, C.S., and Tuan, W.H. (2000) Microstructural evolution of mullite during the sintering of kaolin powder compacts. *Ceramics International*, **26**, 715–720.

Cultrone, G., Rodriguez-Navarro, C., Sebastian, E., Cazalla, O., and De La Torre, M.J., (2001) Carbonate and silicate phase reactions during ceramic firing. *European Journal of Mineralogy*, **13**, 621–634.

Dias, M.I., Viegas, C., Gouveia, M.A., Marques, R., Franco, D., and Prudêncio, M.I. (2009) Geochemical fingerprinting of Roman pottery production from Manta Rota kilns (southern Portugal). Pp. 83–91 in: *Separate monograph of the Hungarian National Museum* (K.T. Biró, V. Szilágyi, and A. Kreiter, editors). Hungarian National Museum, Hungary.

Duminuco, P., Messiga, B., and Riccardi, M.P. (1998) Firing process of natural clays. Some microtextures and related phase compositions. *Thermochimica Acta*, **321**, 185–190.

Fabião, C. (2004) Centros oleiros da Lusitania: balanço dos conhecimentos e perspectivas de investigação. Pp. 379–410 in: *Actas del Congreso Internacional Figlinae Baeticae. Talleres alfareros y producciones cerámicas en la Bética romana (ss. II a.C – VII d.C.)* (D. Bernal and L. Lagóstena, editors). BAR 1266, Oxford, UK.

Ferrari, S. and Gualtieri, A.F. (2006) The use of illitic clays in the production of stoneware tile ceramics. *Applied Clay Science*, **32**, 73–81.

Galhano, C., Rocha, F., and Gomes, C. (1999) Geostatistical analysis of the influence of textural, mineralogical and geochemical parameters on the geotechnical behaviour of the 'Argilas de Aveiro' formation (Portugal). *Clay Minerals*, **34**, 109–116.

Grapes, R. (2006) *Pyrometamorphism*. Springer-Verlag, Berlin, 275 pp.

Jordán, M.M., Sanfeliu, T., and De la Fuente, C. (2001) Firing transformations of Tertiary clays used in the manufacturing of ceramic tile bodies. *Applied Clay Science*, **20**, 87–95.

Kacim, S. and Hajjaji, M. (2003) Firing transformations of a carbonatic clay from the High-Atlas, Morocco. *Clay Minerals*, **38**, 361–365.

Maggetti, M. (1982) Phase analysis and its significance for technology and origin. Pp. 121–133 in: *Archaeological Ceramics* (J.S. Olin, editor). Smithsonian Institution Press, Boston, USA.

Maia, M. (1979) As ânforas de S. Bartolomeu de Castro Marim. *Clio*, **1**, 141–154.

Maniatis, Y., Simopoulos, A., and Kostikas, A. (1983) Effect of reducing atmosphere on minerals and iron oxides developed in fired clays: the role of Ca. *Journal of the American Ceramic Society*, **66**, 773–781.

Martin-Pozas, J.M. (1968) El analisis mineralógico cuantitativo de los filosilicatos de la arcilla por difracción de rayos X. PhD thesis, University of Granada, Spain.

Martins, L. (1991) Actividade ígnea mesozóica em Portugal (contribuição petrológica e geoquímica). PhD thesis, University of Lisbon, Portugal, 418 pp.

Martins, L. and Kerrich, R. (1998) Magmatismo toleítico continental no Algarve (Sul de Portugal): Um exemplo de contaminação crustal "in situ". *Comunicações do Instituto Geológico e Mineiro*, **85**, 99–116.

Miyashiro, A. (1994) *Metamorphic Petrology*. UCL Press, London, 416 pp.

Moropoulou, A., Bakolas, A., and Bisbikou, K. (1995) Thermal analysis as a method of characterizing ancient ceramic technologies. *Thermochimica Acta*, **2570**, 743–753.

Moura, D., Veiga-Pires, C., Albardeiro, L., Boski, T., Rodrigues, A.L., and Tareco, H. (2007) Holocene sea level fluctuations and coastal evolution in the central Algarve (southern Portugal). *Marine Geology*, **237**, 127–142.

Munhá, J. (1990) Metamorphic evolution of the south Portuguese Zone/Pulo do Lobo Zone. Pp. 363–368 in: *Pre-Mesozoic Geology of Iberia* (R.D. Dallmeyer and E. Martínez García, editors). Springer-Verlag, Berlin.

Murad, E. and Wagner, U. (1998) Clays and clay minerals: the firing process. *Hyperfine Interactions*, **117**, 337–356.

Okada, K. and Otsuka, N. (1986) Characterization of spinel phase from $SiO_2$-$Al_2O_3$ xerogels and the formation process of mullite. *Journal of the American Ceramic Society*, **69**, 652–656.

Oliveira, A., Rocha, F., Rodrigues, A., Jouanneau, J., Dias, A., Weber, O., and Gomes, C. (2002) Clay minerals from the sedimentary cover from the Northwest Iberian shelf. *Progress in Oceanography*, **52**, 233–247.

Oliveira, J.T. (1990) Stratigraphy and synsedimentary tectonism. Pp. 334–347 in: *Pre-Mesozoic Geology of Iberia* (R.D. Dallmeyer and E. Martínez García, editors). Springer-Verlag, Berlin.

Önal, M., Yilmaz, H., and Sarikaya, Y. (2008) Some physicochemical properties of the white sepiolite known as pipestone from Eskişehir, Turkey. *Clays and Clay Minerals*, **56**, 511–519.

Peters, T. and Iberg, R. (1978) Mineralogical changes during firing of calcium-rich brick clays. *Ceramic Bulletin*, **57**, 503–509.

Riccardi, M.P., Messiga, B., and Duminuco, P. (1999) An approach to the dynamics of clay firing. *Applied Clay Science*, **15**, 393–409.

Rice, P.M. (1987) *Pottery Analysis: A Sourcebook*. University of Chicago Press, Chicago, USA, 559 pp.

Schultz, L.G. (1964) Quantitative interpretation of mineralogical composition from X-ray and chemical data for the Pierre Shale. *United States Geological Survey, Professional Paper*, **391-C**, 1–31.

Terrinha, P. (1998) Structural geology and tectonic evolution of the Algarve basin, south Portugal. PhD thesis, Imperial College London, England.

Terrinha, P., Rocha, R., Rey, J., Cachão, M., Moura, D., Roque, C., Martins, L., Valadares, V., Cabral, J., Azevedo, M.R., Barbero, L., Clavijo, E., Dias, R.P., Gafeira, J., Matias, H., Matias, L., Madeira, J., Marques da Silva, C., Munhá, J., Rebelo, L., Ribeiro, C., Vicente, J., and Youbi,

N. (2006) A Bacia do Algarve: Estratigrafia, paleogeografia e tectónica. Pp. 247−316 in: *Geologia de Portugal no contexto da Ibéria* (R. Dias, A. Araújo, P. Terrinha and J.C. Kullberg, editors). University of Évora, Portugal.

Traoré, K., Kabré, T.S., and Blanchart, P. (2000) Low temperature sintering of a pottery clay from Burkina Faso. *Applied Clay Science*, **17**, 279−292.

Traoré, K., Kabré, T.S., and Blanchart, P. (2003) Gehlenite and anorthite crystallization from kaolinite and calcite mix. *Ceramics International*, **29**, 377−383.

Trindade, M.J.F. (2007) Geoquímica e mineralogia de argilas da Bacia Algarvia: transformações térmicas. PhD thesis, University of Aveiro, Portugal, 440 pp.

Trindade, M.J., Dias, M.J., Coroado, J., and Rocha, F. (2009) Mineralogical transformations of calcareous rich clays with firing: A comparative study between calcite and dolomite rich clays from Algarve (Portugal). *Applied Clay Science*, **42**, 345−355.

Vasconcellos, J.L. (1898) Olaria luso-romana em S. Bartolomeu de Castro Marim. *O Arqueólogo Português*, **4**, 329−336.

Vasconcellos, J.L. (1920) A olaria Lusitano-romana (?) de Manta Rôta. *O Arqueólogo Português*, **24**, 229.

Velde, B. and Druc, I.C. (1999) *Archaeological Ceramic Materials: Origin and Utilization*. Springer, Berlin, 299 pp.

Viegas, C. (2006) O Forno romano da Manta Rota (Algarve). Pp. 177−196 in: *Produção e comércio de Preparados Piscícolas durante a Proto-História e a Época Romana no Ocidente da Península Ibérica*. Setúbal Arqueológica, **13**, Actas do Simpósio Internacional de Homenagem a Françoise Mayet, Setúbal, Portugal.

Wahl, F.M., Grim, R.E., and Graf, R.B. (1961) Phase transformations in silica as examined by continuous X-ray diffraction. *American Mineralogist*, **46**, 196−208.